Kinetic Studies of Temperature Anisotropy Instability in Intense Charged Particle Beams*

Edward A. Startsev and Ronald C. Davidson and Hong Qin
Plasma Physics Laboratory, Princeton University, Princeton, New Jersey 08543

Abstract

This paper extends previous analytical and numerical studies [E. A. Startsev, R. C. Davidson and H. Qin, *Phys. Plasmas* **9**, 3138 (2002)] of the stability properties of intense nonneutral charged particle beams with large temperature anisotropy $\left(T_{\perp b} \gg T_{\| b}\right)$ to allow for non-axisymmetric perturbations with $\partial/\partial\theta \neq 0$. The most unstable modes are identified, and their eigenfrequencies and radial mode structure are determined.

LINEAR STABILITY THEORY

It is well known that in neutral plasmas with strongly anisotropic distributions $(T_{||b}/T_{\perp b} \ll 1)$ a collective Harris instability [1] may develop if there is sufficient coupling between the transverse and longitudinal degrees of freedom. Such anisotropies develop naturally in accelerators. For particles with charge q accelerated by a voltage V, the longitudinal temperature decreases according to $T_{||bf} = T_{||bi}^2/2qV$ (for a nonrelativistic beam). At the same time, the transverse temperature may increase due to nonlinearities in the applied and self-field forces, nonstationary beam profiles, and beam mismatch. These processes may provide the free energy to drive collective instabilities, and lead to a detoriation of beam quality. The instability may also result in an increase in the longitudinal velocity spread, which will make the focusing of the beam difficult, and may impose a limit on the minimum spot size achievable in heavy ion fusion experiments.

We briefly outline here a simple derivation [2] of the Harris-like instability in intense particle beams for electrostatic perturbations about the thermal equilibrium distribution with temperature anisotropy $(T_{\perp b} > T_{\| b})$ described *in the beam frame* by the self-consistent axisymmetric Vlasov equilibrium [3]

$$f_b^0(r,\mathbf{p}) = \frac{\widehat{n}_b}{(2\pi m_b)^{3/2} T_{\perp b} T_{\| b}^{1/2}} \exp\left(-\frac{H_\perp}{T_{\perp b}} - \frac{H_\|}{T_{\| b}}\right). \tag{1}$$

Here, $H_\| = p_z^2/2m_b$, $H_\perp = p_\perp^2/2m_b + (1/2)m_b\omega_f^2 r^2 + e_b\phi^0(r)$ is the single-particle Hamiltonian for transverse particle motion, $p_\perp = (p_x^2 + p_y^2)^{1/2}$ is the transverse particle momentum, $r = (x^2+y^2)^{1/2}$ is the radial distance from the beam axis, $\omega_f = const.$ is the transverse frequency associated with the applied focusing field in the smooth-focusing approximation, and $\phi^0(r)$ is the equilibrium space-charge potential determined self-consistently from Poisson's equation,

$$\frac{1}{r}\frac{\partial}{\partial r} r \frac{\partial \phi^0}{\partial r} = -4\pi e_b n_b^0, \tag{2}$$

where $n_b^0(r) = \int d^3p f_b^0(r,\mathbf{p})$ is the equilibrium number density of beam particles. A perfectly conducting wall is located at radius $r = r_w$.

For present purposes, we consider small-amplitude electrostatic perturbations of the form

$$\delta\phi(\mathbf{x},t) = \widehat{\delta\phi}(r)\exp(im\theta + ik_z z - i\omega t), \tag{3}$$

where $\delta\phi(\mathbf{x},t)$ is the perturbed electrostatic potential, k_z is the axial wavenumber, m is the azimuthal mode number and ω is the complex oscillation frequency, with $Im\omega > 0$ corresponding to instability (temporal growth). Without presenting algebraic details, using the method of characteristics [2, 3], the linearized Poisson equation can be expressed as

$$\left(\frac{1}{r}\frac{\partial}{\partial r} r \frac{\partial}{\partial r} - k_z^2 - \frac{m^2}{r^2}\right)\widehat{\delta\phi}(r) = -4\pi e_b \int d^3p \widehat{\delta f_b}, \tag{4}$$

where

$$\widehat{\delta f_b} = e_b \frac{\partial f_b^0}{\partial H_\perp}\widehat{\delta\phi} + e_b\left[(\omega - k_z v_z)\frac{\partial f_b^0}{\partial H_\perp} + k_z v_z \frac{\partial f_b^0}{\partial H_{||}}\right]$$
$$\times i \int_{-\infty}^{t} dt' \widehat{\delta\phi}[r'(t')] \exp[i(k_z v_z - \omega)(t'-t) + im\theta'(t')], \tag{5}$$

for perturbations about the choice of the anisotropic thermal equilibrium distribution function in Eq. (1). In the orbit integral in Eq. (5), $Im\omega > 0$ is assumed, and $r'(t') = [x'^2(t') + y'^2(t')]^{1/2}$ and $\theta'(t')$ are the transverse orbits in the equilibrium field configuration such that $[\mathbf{x}'_\perp(t'), \mathbf{p}'_\perp(t')]$ passes through the phase-space point $(\mathbf{x}_\perp, \mathbf{p}_\perp)$ at time $t' = t$ [2, 3].

In Eq. (4), we express the perturbation amplitude as $\widehat{\delta\phi}(r) = \sum \alpha_n \phi_n(r)$, where $\{\alpha_n\}$ are constants, and the complete set of vacuum eigenfunctions $\{\phi_n(r)\}$ is defined by $\phi_n(r) = A_n J_m(\lambda_n r/r_w)$. Here, λ_n is the n'th zero of Bessel function $J_m(\lambda_n) = 0$, and A_n is a normalization constant [2]. This gives the matrix dispersion equation

$$\sum_n \alpha_n D_{n,n'}(\omega) = 0. \tag{6}$$

The condition for a nontrivial solution to Eq. (6) is

$$det\{D_{n,n'}(\omega)\} = 0, \tag{7}$$

* Research supported by the U. S. Department of Energy

which plays the role of a matrix dispersion relation that determines the complex oscillation frequency ω [2].

In the present analysis, it is convenient to introduce the effective *depressed* betatron frequency $\omega_{\beta\perp}$. It can be shown [3] for the equilibrium distribution in Eq. (1), that the mean-square beam radius $r_b^2 = \langle r^2 \rangle = N_b^{-1} 2\pi \int_0^{r_w} dr r^3 n_b^0(r)$ is related *exactly* to the line density $N_b = 2\pi \int_0^{r_w} dr r n_b^0(r)$, and the transverse beam temperature $T_{\perp b}$, by the equilibrium radial force balance equation

$$\omega_f^2 r_b^2 = \frac{N_b e_b^2}{m_b} + \frac{2T_{\perp b}}{m_b}. \tag{8}$$

Equation (8) can be rewritten as

$$\left(\omega_f^2 - \frac{1}{2}\bar{\omega}_{pb}^2\right) r_b^2 = \frac{2T_{\perp b}}{m_b}, \tag{9}$$

where we have introduced the effective *average* beam plasma frequency $\bar{\omega}_{pb}$ defined by

$$r_b^2 \bar{\omega}_{pb}^2 \equiv \int_0^{r_w} dr r \omega_{pb}^2(r) = \frac{2e_b^2 N_b}{m_b}, \tag{10}$$

where $\omega_{pb}^2(r) = 4\pi n_b^0(r) e_b^2/\gamma_b m_b$ is the relativistic plasma frequency-squared. Then, Eq. (9) can be used to introduce the effective *depressed* betatron frequency $\omega_{\beta\perp}$ defined by

$$\omega_{\beta\perp}^2 \equiv \left(\omega_f^2 - \frac{1}{2}\bar{\omega}_{pb}^2\right) = \frac{2T_{\perp b}}{m_b r_b^2}, \tag{11}$$

and the normalized tune depression $\bar{\nu}/\nu_0$ defined by

$$\frac{\bar{\nu}}{\nu_0} \equiv \frac{\omega_{\beta\perp}}{\omega_f} = (1 - \bar{s}_b)^{1/2}. \tag{12}$$

If, for example, the beam density were uniform over the beam cross section, then Eq. (11) corresponds to the usual definition of the depressed betatron frequency for a Kapchinskij – Vladimirskij (KV) [3] beam, and it is readily shown that the radial orbit $\widehat{r}(\tau)$ occurring in Eq. (5) can be expressed as [2]

$$\widehat{r}^2(\tau) = \frac{H_\perp}{m_b \omega_{\beta\perp}^2}\left[1 - \sqrt{1 - \left(\frac{\omega_{\beta\perp} P_\theta}{H_\perp}\right)^2} \cos(2\omega_{\beta\perp}\tau)\right]. \tag{13}$$

In general, for the choice of equilibrium distribution function in Eq. (1), there will be a spread in transverse depressed betatron frequencies $\omega_{\beta\perp}(H_\perp, P_\theta)$, and the particle trajectories will not be described by the simple trigonometric function in Eq. (13). For present purposes, however, we consider a simple *model* in which the radial orbit $\widehat{r}(\tau)$ occurring in Eq. (5) is approximated by Eq. (13) with the constant frequency $\omega_{\beta\perp}$ defined in Eq. (11), and the approximate equilibrium density profile is defined by $n_b^0(r) = \widehat{n}_b \exp(-m_b \omega_{\beta\perp}^2 r^2/2T_{\perp b})$. For a nonuniform beam, $\omega_{\beta\perp}^{-1}$ is the characteristic time for a particle with thermal speed $v_{th\perp} = (2T_{\perp b}/m_b)^{1/2}$ to cross the rms radius r_b of the beam. In this case $D_{n,n'}(\omega)$ can be evaluated in closed analytical form [2] provided the conducting wall is sufficiently far removed from the beam ($r_w/r_b \geq 3$, say). In this case, the matrix elements decrease exponentially away from the diagonal, with

$$\left|\frac{D_{n,n+k}}{D_{n,n}}\right| \sim \exp\left(-\frac{\pi^2 k^2}{4}\frac{r_b^2}{r_w^2}\right), \tag{14}$$

where k is an integer. Therefore, for $r_w/r_b \geq 3$, we can approximate $\{D_{n,n'}(\omega)\}$ by a *tri-diagonal* matrix. In this case, for the lowest-order radial modes ($n = 1$ and $n = 2$), the dispersion relation (7) can be approximated by [2]

$$D_{1,1}(\omega)D_{2,2}(\omega) - [D_{1,2}(\omega)]^2 = 0, \tag{15}$$

where use has been made of $D_{1,2}(\omega) = D_{2,1}(\omega)$.

Typical numerical results [2] obtained from the approximate dispersion relation utilizing Eq. (15) are presented in Figs. 1 – 2 for the case where $r_w = 3r_b$. Only the leading-order nonresonant terms and one resonant term at frequencies $\omega \approx \pm 2\omega_{\beta\perp}$ for even values of m, and $\omega \approx \pm\omega_{\beta\perp}$ for odd values of m, have been retained in the analysis [2]. Note from Fig. 1 that the critical values of $k_z r_w$ for the onset of instability and for maximum growth rate increase as the azimuthal mode number m is increased. As expected, finite – $T_{\|b}$ effects introduce a finite bandwidth in $k_z r_w$ for instability, since the modes with large values of $k_z r_w$ are stabilized by Landau damping [2, 3]. Also, the unstable modes with odd azimuthal number are purely growing.

Note from Fig. 2 that the $m = 1$ dipole mode has the

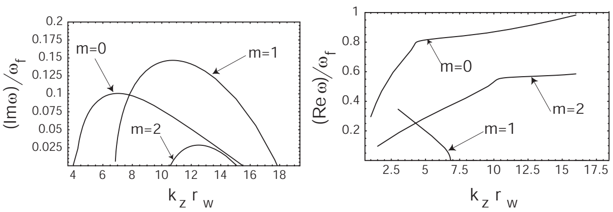

Figure 1: Plots of normalized growth rate $(Im\omega)/\omega_f$ and real frequency $(Re\omega)/\omega_f$ versus $k_z r_w$ for $\bar{\nu}/\nu_0 = 0.53$ and $T_{||b}/T_{\perp b} = 0.02$ [2].

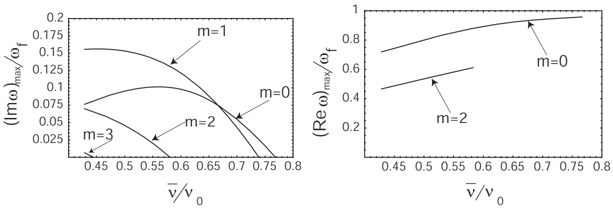

Figure 2: Plots of normalized growth rate $(Im\omega)_{max}/\omega_f$ and real frequency $(Re\omega)_{max}/\omega_f$ at maximum growth versus tune depression $\bar{\nu}/\nu_0$ for $T_{||b}/T_{\perp b} = 0.02$ [2].

highest growth rate, $(Im\omega)/\omega_f \simeq 0.15$, for $\bar{\nu}/\nu_0 \simeq 0.45$, and that the critical value of $\bar{\nu}/\nu_0$ for the onset of the instability, and the value of $(\bar{\nu}/\nu_0)^{max}$ with maximum growth rate, decrease with azimuthal mode number m. The instability is absent for $\bar{\nu}/\nu_0 > 0.77$ for the choice of parameters in Fig. 2. The real frequency $(Re\omega)/\omega_f$ of the unstable modes with odd azimuthal numbers $m = 1, 3, \cdots$ are zero and are not plotted in Fig. 2. Moreover, the real frequency is plotted only for the unstable modes.

BEST SIMULATION RESULTS

Typical numerical results obtained with the *linearized* version of the 3D BEST code [4] are presented in Figs. 3-5 [2] for the case where $r_w = 3r_b$ and $T_{||b}/T_{\perp b} = 0.02$, and for perturbations with a spatial dependence proportional to $\exp(ik_z z + im\theta)$, where k_z is the axial wavenumber, and m is the azimuthal mode number. Random initial perturbations are introduced to the particle weights, and the beam is propagated from $t = 0$ to $t = 200\omega_f^{-1}$. Note from Fig.

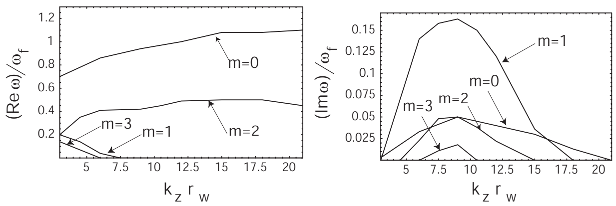

Figure 3: Plots of normalized real frequency $(Re\omega)/\omega_f$ and growth rate $(Im\omega)/\omega_f$ versus $k_z r_w$ for $\bar{\nu}/\nu_0 = 0.53$ and $T_{||b}/T_{\perp b} = 0.02$ [2].

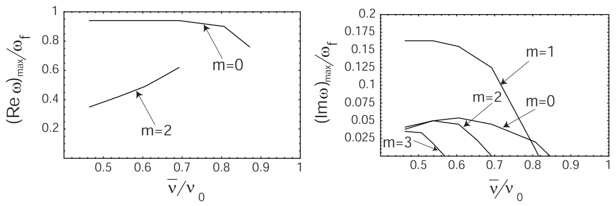

Figure 4: Plots of normalized real frequency $(Re\omega)_{max}/\omega_f$ and growth rate $(Im\omega)_{max}/\omega_f$ at maximum growth versus normalized tune depression $\bar{\nu}/\nu_0$ for $T_{||b}/T_{\perp b} = 0.02$ [2].

3 that the instability has a finite bandwidth with maximum growth rate occurring at $k_z r_w \simeq 9$. From Fig. 4, the critical value of $\bar{\nu}/\nu_0$ for the onset of the instability decreases with azimuthal mode number m. The real frequency $(Re\omega)/\omega_f$ of the unstable modes for odd azimuthal numbers $m = 1, 3$ are zero and are not plotted. Moreover, the real frequency is plotted only for the unstable modes. Consistent with the analytical predictions, note that the dipole mode ($m = 1$) has the largest growth rate. Furthermore, all modes are found to be stable in the region $\bar{\nu}/\nu_0 \geq 0.85$. The simulation results presented in Figs. 3 and 4 are in good qualitative agreement with the theoretical model (see Figs. 1 and 2). Moreover, Fig. 5 shows that instability is absent for $T_{\|b}/T_{\perp b} > 0.08$.

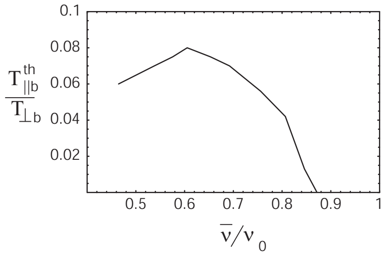

Figure 5: Longitudinal threshold temperature $T_{||b}^{th}$ normalized to the transverse temperature $T_{\perp b}$ for onset of instability plotted versus normalized tune depression $\bar{\nu}/\nu_0$ [2].

CONCLUSIONS

To summarize, the BEST code [4] was used to investigate the detailed stability properties of intense charged particle beams with large temperature anisotropy ($T_{||b}/T_{\perp b} \ll 1$) for three-dimensional perturbations with several values of azimuthal wave number $m = 0, 1, 2, 3$. An analytical model, which generalizes the classical Harris-like instability to the case of an intense charged particle beam with anisotropic temperature, has been developed [2]. Both the simulations and the analytical results clearly show that moderately intense beams with $s_b \geq 0.5$ are linearly unstable to short wavelength perturbations with $k_z^2 r_b^2 \geq 1$, provided the ratio of longitudinal and transverse temperatures is smaller than some threshold value.

REFERENCES

[1] E. G. Harris, Phys. Rev. Lett. **2**, 34 (1959).

[2] E. A. Startsev, R. C. Davidson and H. Qin, Phys. Plasmas **10** submited (2003); Phys. Plasmas **9**, 3138 (2002);

[3] R. C. Davidson and H. Qin, *Physics of Intense Charged Particle Beams in High Energy Accelerators* (World Scientific, Singapore, 2001), and references therein.

[4] H. Qin, R. C. Davidson and W. W. Lee, Phys. Rev. Special Topics on Accelerators and Beams **3**, 084401 (2000); **3**, 109901 (2000).